Supplementary Material

Impact of exposed crystal facets on oxygen reduction reaction activity in zeolitic imidazole framework

Sorawich Pimu[a†], Nuttapon Yodsin[b†], Sirawee Maneewan[a], Jaruwan Kanthachan[a], Supawadee Namuangruk[b,*] and Kanokwan Kongpatpanich[a,*]

[a]*Department of Materials Science and Engineering, School of Molecular Science and Engineering, Vidyasirimedhi Institute of Science and Technology, Rayong 21210, Thailand. Email: kanokwan.k@vistec.ac.th*

[b]*National Nanotechnology Center (NANOTEC), National Science and Technology Development Agency (NSTDA), Pathum Thani 12120, Thailand. Email: supawadee@nanotec.or.th*

† *Both authors contributed equally to this work*

S1. Methodology

Experimental section

1. Chemicals

$Co(NO_3)_2 \cdot 6H_2O$ (≥99%, Merck), $Co(OAc)_2 \cdot 4H_2O$ (≥98%, Sigma-Aldrich), 2-methylimamdazole (99%, Sigma-Aldrich), cetyltrimethylammonium bromide (≥98%, Sigma-Aldrich), carbon black, super P conductive (≥99%, Alfa aesar), nafion perfluorinated resin solution (5 wt% in mixture of lower aliphatic alcohols and water, contains 45% water, Merck), platinum, nominally 20% on carbon black (Alfa aesar), ethanol (99.9%, AR grade, Qrec), methanol (99.8%, AR grade, Qrec), Deionized water (Millipore Milli-Q grade). All of the chemicals used in this experiment were used as received without any further purification.

2. Synthesis methods

Snthesis of ZIF-67 (100)

$Co(NO_3)_2 \cdot 6H_2O$ (292 mg) and cetyltrimethylammonium bromide (4 mg) were dissolved in 10 mL of DI water (solution A). Then, the solution of 2-methylimidazole (4.54 g) in DI water (70 mL) (solution B) was rapidly added into solution A under stirring until homoginized. The mixture solution was kept at room temperature for 40 min. The purple powder was collected by centrifugation, washed with ethanol and dried at 80 °C overnight.

Synthesis of ZIF-67 (110)

$Co(NO_3)_2 \cdot 6H_2O$ (1.455 g) was dissolved in the 1:1 mixture of methanol and ethanol (80 mL) (solution A). 2-methylimidazole (1.642 g) was dissolved in another 1:1 mixture of methanol and ethanol (80 mL). Then, the solution A and B were mixed under stirring until homoginized. The mixture solution was kept at room temperature for 24 h. The purple powder was collected by centrifugation, washed with ethanol and dried at 80 °C overnight.

Synthesis of bulk ZIF-67

$Co(OAc)_2$ (1.2 g) in DI water (10 mL) (solution A) was added into a solution of 2-methylimidazole (4.48 g) in DI water (10 mL) (solution B) under stirring until homoginized. The mixture solution was kept at room temperature for 15 min. The purple powder was collected by centrifugation, washed with methanol and dried at 80 °C overnight.

3. Materials characterization

Scanning electron microscopy (SEM) images were collected by JEOL JSM-7610F. The X-ray diffraction (XRD) was performed by a Bruker D8 ADVANCE X-ray diffractometer using Cu *Kα* radiation (40 kV, 40 mA, λ = 1.5418 Å). Nitrogen (N_2) adsorption experiments were determined with a MicrotracBEL BELSORP-mini II at -196 ℃. All samples were activated at 140 ℃ for 12 hours before gas adsorption experiments. Bruauer-Emmett-Teller (BET) method was used to calculate the surface area. The chemical environment was identified using X-ray photoelectron spectroscopy (XPS) data recorded on a JEOL JPS-9010MC with Mg K*α* source (12 kV, 25 mA) and under a high vacuum pressure (10^{-7} Pa). All binding energy values were referenced to the C 1s peak (284.70 eV). All electrochemical analyses were performed on an Autolab PGSTAT302N, Metrohm. The ^{1}H nuclear magnetic resonance (^{1}H NMR) spectra were recorded on a Bruker D8 AVANCE III HD (600 MHz) at room temperature. To digest the samples, 10 mg of MOF was soaking in the mixture of 15 mL 2%H_2SO_4, and 5 mL H_2O_2 for 24 h. The filtrate solution (300 μL) was mixed with DMSO-d_6 (300 μL) for NMR measurement.

4. Electrochemical measurements

The electrocatalytic activity of each sample was tested using a three-electrode system. A glassy carbon rotating disk electrode (GC-RDE, 0.07065 cm^2), platinum rod, and Ag/AgCl (3 M KCl) electrode were employed as the working electrode, counter electrode, and reference electrode, respectively. The catalyst ink was prepared by using the mixture of isopropanol (960 μL) and 5 wt% Nafion solution (40 μL) containing a catalyst (4 mg) and carbon black (4 mg), followed by ultrasonication for 30 min. Then, the catalyst ink (5 μL) was dropped onto the GC-RDE electrode and dried at room temperature for 18 h, so that the catalyst loading is 0.28 $mg \cdot cm^{-2}$. The benchmark 20 wt% Pt/C was used as the reference material and tested under the same catalyst loading. Linear sweep voltammetry (LSV) data were carried out in 0.1 M KOH solution saturated with O_2 at a scan rate of 5 $mV \cdot s^{-1}$ with a rotating speed of 400, 625, 900, 1225, 1600, 2025, and 2500 rpm. The background subtraction was performed under N_2 saturation conditions under the same measurement. Tafel plots were calculated by measuring LSV data at a scan rate of 5 $mV \cdot s^{-1}$ and 1600 rpm rotating speed. Cyclic voltammetry (CV) was performed from 1.00 to 1.10 V (vs RHE) to measure the electrochemical double-layer capacitance (C_{dl}) at a non-faradaic region with variable scan rates of 20, 40, 60, 80, 100, 120, 140, 160, 180, and 200 $mV \cdot s^{-1}$. Stability testing was conducted using the chronoamperometric technique in O_2-saturated

0.1 M KOH electrolyte with a rotation speed of 1600 rpm. All potentials measured from Ag/AgCl were converted to reversible hydrogen electrode (RHE) potentials by using the following Nernst equation

$$E_{RHE} = E_{Ag/AgCl} + 0.059pH + E^0_{Ag/AgCl} \quad (1)$$

The number of electrons (*n*) of the ORR process was calculated by Koutecky-Levich (K-L) equation

$$1/J = 1/J_L + 1/J_K = 1/(B\omega^{1/2}) + 1/(nFkC_0) \quad (2)$$

$$B = 0.2nFC_0D_0^{2/3}v^{-1/6} \quad (3)$$

Where *J* is the current density measured with LSV, J_L and J_K are measured diffusion and kinetic-limiting of current density, B is the slope of K-L plots, ω is the electrode rotating rate (rpm), *n* is the number of electrons transferred per oxygen molecule, F is the Faraday constant (96,485 $C \cdot mol^{-1}$), *k* is the electron transfer rate constant, C_0 is the bulk concentration of O_2 (1.2×10^{-6} $mol \cdot cm^{-3}$), D_0 is the diffusion coefficient of O_2 (1.9×10^{-5} $cm^2 \cdot s^{-1}$), and v is the kinetic viscosity of the electrolyte 0.1 M KOH (0.01 $cm^2 \cdot s^{-1}$). The constant 0.2 is adopted when the rotation speed is expressed in rpm.

5. DFT calculations

The calculations were performed by means of density functional theory (DFT) calculations with the Vienna *ab initio* simulation package (VASP)[1-3]. The electron exchange-correlation was represented by the Perdew–Burke–Ernzerhof (PBE) functional with generalized gradient approximation (GGA)[4]. The interaction between ion cores and valence electrons was ascribed by the projector augmented wave (PAW) method [5], and we used Grimme's dispersion correction (DFT-D3)[6], to account for the van der Waals force. The kinetic energy cut-off for plane wave expansions was set to be 450 eV, and the reciprocal space was sampled by the Γ point. The convergence criteria are 1 x 10^{-5} eV energy differences for the electronic wave function for structure optimization and vibrational frequency calculations. We fixed the catalyst and vibrated adsorbate, then we can collect the vibration frequency of different intermediates. T All atomic coordinates are converged to within 0.02 eV/Å for maximal components of forces.

The computational ZIF-67 bulk unit cell was a cubic cell from experimental crystallographic data.[7] These calculations gave a DFT-optimized lattice constant of 16.708 Å, in agreement with the experimental value (16.908 Å). Moreover, we compared structural

dimensions between simulation and experimental value, i.e., metal-nitrogen distance (D1), metal-metal distance (D2), and approximated pore aperture (PA), as demonstrated in **Figure S5**. Then, we used an optimized bulk ZIF-67 structure to generate a set of surface slab models by cleaving Co−N bonds crossing specified crystal plane. The slab model of (100) surfaces was modeled with truncations and a vacuum region of at least 16 Å to avoid the interaction with neighboring periodic cells. The simulation cell sizes of each facet are depicted in **Figure S6 and S7**. A four-layer slab in which the bottom two layers were fixed in bulk positions and the top two layers were allowed to relax was chosen to mimic the surface. In addition, the surface energy was investigated to clarify the most stable surface facets. The surface energy of the slab is defined as

$$E_s = \frac{1}{A}(E_{slab} - E_{bulk})$$

where A is the area of surface, E_{slab} is the energy of a slab, and E_{bulk} is the energy of bulk. By comparing the surface energy of all possible surface terminations, we have found that there are two possible (100) surface terminations, and the one that Co^{2+} atom coordinates to two imidazolates (E_s = 0.55 J/m^2) is much more stable rather than it is three imidazolates coordination (E_s = 1.19 J/m^2). In the case of (110) surfaces, we found only three imidazolates coordination as demonstrated in **Figure S6**.

ORR can normally take place in two ways: in a two-step 2e- pathway that reduces O_2 to H_2O_2, or in a direct 4e- process that reduces O_2 to H_2O directly. The associative 4e- reaction, each elementary reactions in basic condition in this study are (4) - (7)

$$* + O_2 + H_2O + e^- \rightarrow *OOH + OH \quad (4)$$

$$*OOH + OH^- + e^- \rightarrow *O + 2OH^- \quad (5)$$

$$*O + H_2O + e^- \rightarrow *OH + OH^- \quad (6)$$

$$*OH + OH^- + e^- \rightarrow * + 2OH^- \quad (7)$$

The ORR of 2 e mechanism comprises of elementary steps (8) and (9):

$$* + O_2 + H_2O + e- \rightarrow *OOH + OH^- \quad (8)$$

$$*OOH + OH- + H_2O + e^- \rightarrow * + H_2O_2 + 2OH^- \quad (9)$$

Therefore, the DFT adsorption energies of OOH*, O*, and OH* are calculated relative to H_2O and H_2 molecular energies according to the following equations (10) - (12)

$$\Delta E_{ads}(OOH^*) = E_{OOH^*} - E^* - (2G_{H2O} - 3/2G_{H2}) \quad (10)$$

$$\Delta E_{ads}(O^*) = E_{OH^*} - E^* - (G_{H2O} - G_{H2}) \quad (11)$$

$$\Delta E_{ads}(OH^*) = E_{OH^*} - E^* - (G_{H2O} - 1/2G_{H2}) \quad (12)$$

The Gibbs free energy (G) of the intermediates can be calculated as:

$$G = \Delta Eads + \Delta E_{ZPE} - T\Delta S + \int C_p dT + G_U \quad (13)$$

where $\Delta Eads$ is calculated from equations (10) - (12), ΔE_{ZPE}, $T\Delta S$, and $\int C_p dT$ referred to the change in zero-point energies, the change in entropy at temperature T, and the enthalpic temperature correction. The Gibbs free energies of gas-phase molecules are calculated from **Table S3**. We corrected by the vibrational frequency calculations at 298.15 K. ΔG_U represent the change in the difference in electrode potential of the electrochemical ORR reaction, which can be calculated by $\Delta G_U = -neU$, where n, e and U are the number of transferred electrons, the electron charge, and applied potential to the reaction, accordingly. When the there is no applied potential in the reaction, the ΔG_U is zero.

The Gibbs free energy changes (ΔG) of each ORR step on ZIF-67 are calculated by the following equations:

$$\Delta G1 = G_{OOH^*} - 4.92\ eV \quad (14)$$

$$\Delta G2 = G_{O^*} - G_{OOH^*} \quad (15)$$

$$\Delta G3 = G_{OH^*} - G_{O^*} \quad (16)$$

$$\Delta G4 = G_{OH^*} \quad (17)$$

Because DFT methods cannot precisely compute the energy of the triplet O_2 molecule, the Gibbs free energy of O_2 is then set as 4.92 eV from the formation free energy of two water molecules: $2H_2O \rightarrow O_2 + 2H_2$. The Gibbs free energy of each intermediate state of the ORR reactions is performed following the computational hydrogen electrode (CHE) method suggested by Nørskov et al.[8], which approximate the free energy of a proton and an electron by half the free energy of a hydrogen molecule at U = 0 V vs. RHE.

Additionally, the overpotential (η) are important factors for evaluating the catalytic activity, the minimum ORR overpotential η^{ORR} can be defined as:

$$\eta^{ORR} = 1.23V - \min(\Delta G_1, \Delta G_2, \Delta G_3, \Delta G_4)/e \quad (18)$$

Specifically, an ideal electrocatalyst requires all ΔG_i approximately 1.23 eV to confirm that the ORR can spontaneously proceed just above the equilibrium potential.

S2. Additional results

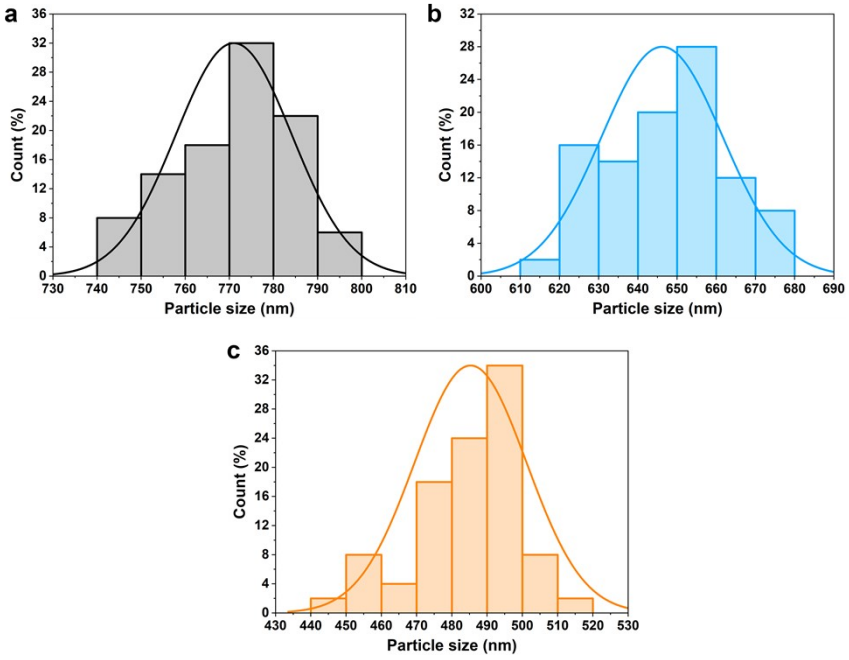

Fig. S1 Particle size distribution of (a) bulk (b) rhombic and (c) cubic ZIF-67.

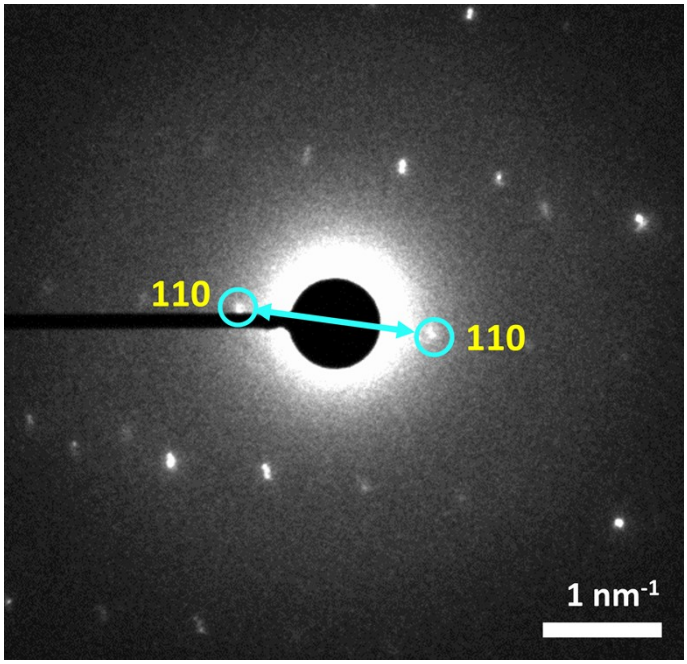

Fig. S2 SAED image of ZIF-67 rhombic.

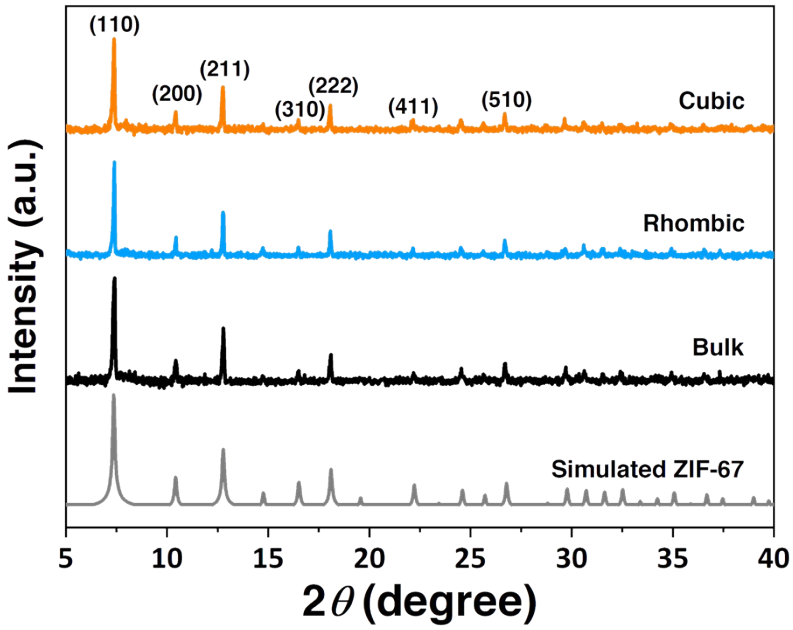

Fig. S3 XRD patterns of all ZIF-67 samples compared to the simulated pattern of ZIF-67.

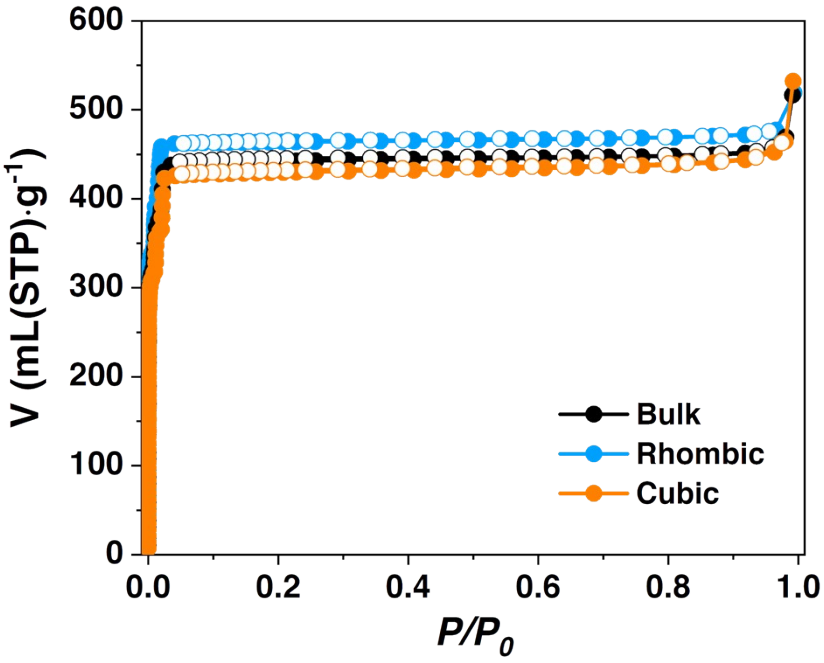

Fig. S4 N_2 adsorption isotherms of all ZIF-67 sample.

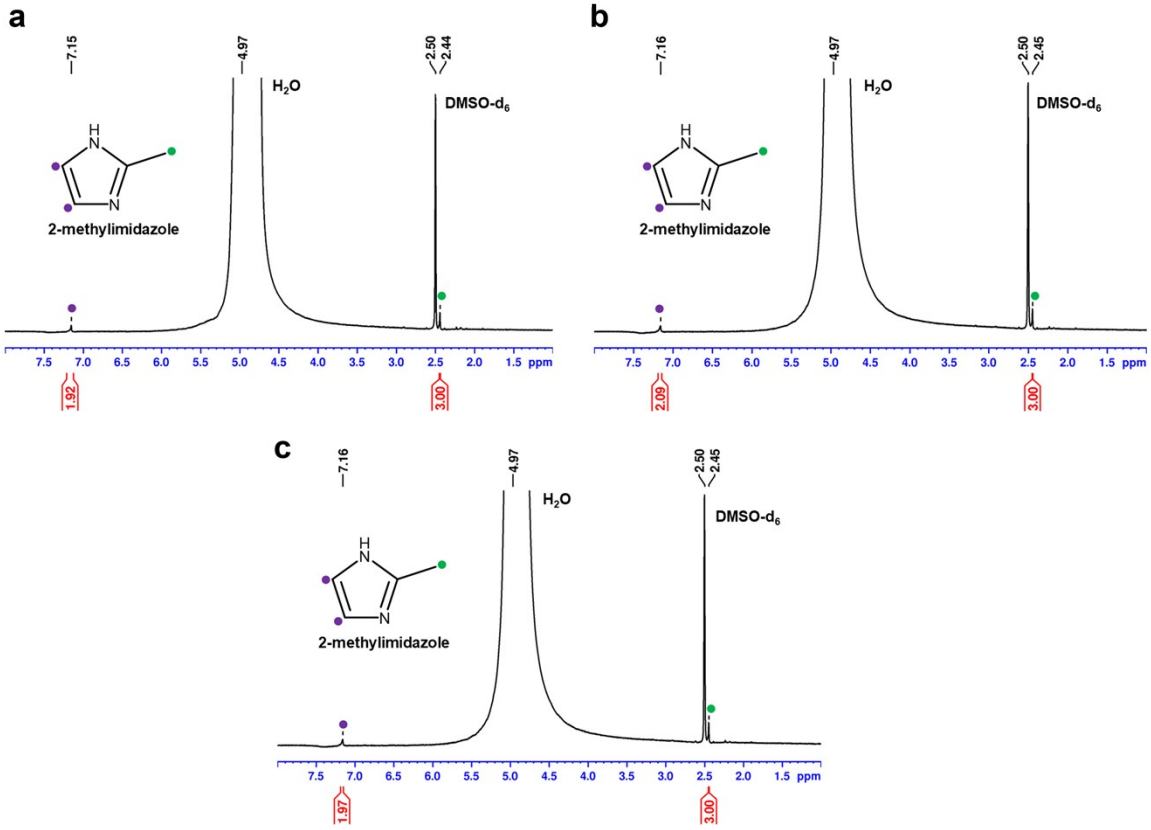

Fig. S5 [1]H-NMR spectra of the digested ZIF-67 samples after soaking of (a) bulk (b) rhombic and (c) cubic.

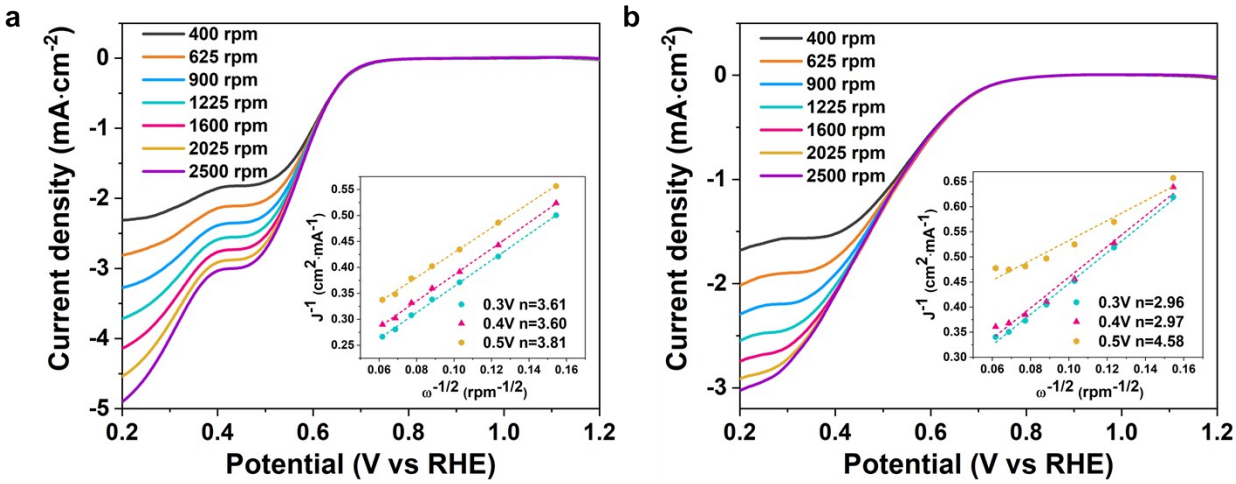

Fig. S6 Electron transfer number of ZIF-67 (a) bulk and (b) rhombic.

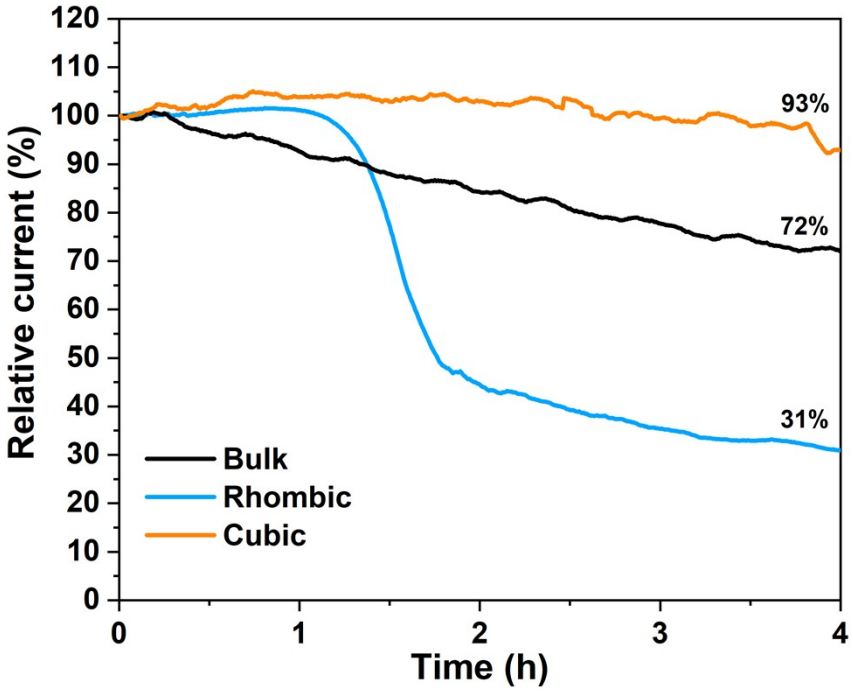

Fig. S7 Stability test of all ZIF-67 samples at 0.46 V (vs RHE) and 1600 rpm in O_2-saturated 0.1 M KOH solution.

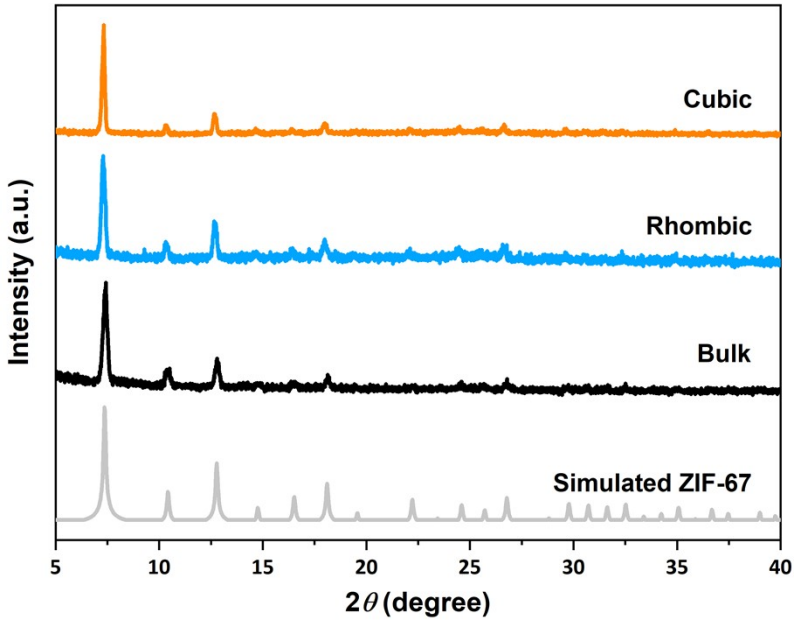

Fig. S8 XRD patterns of all ZIF-67 samples after ORR performance compared to the simulated pattern of ZIF-67.

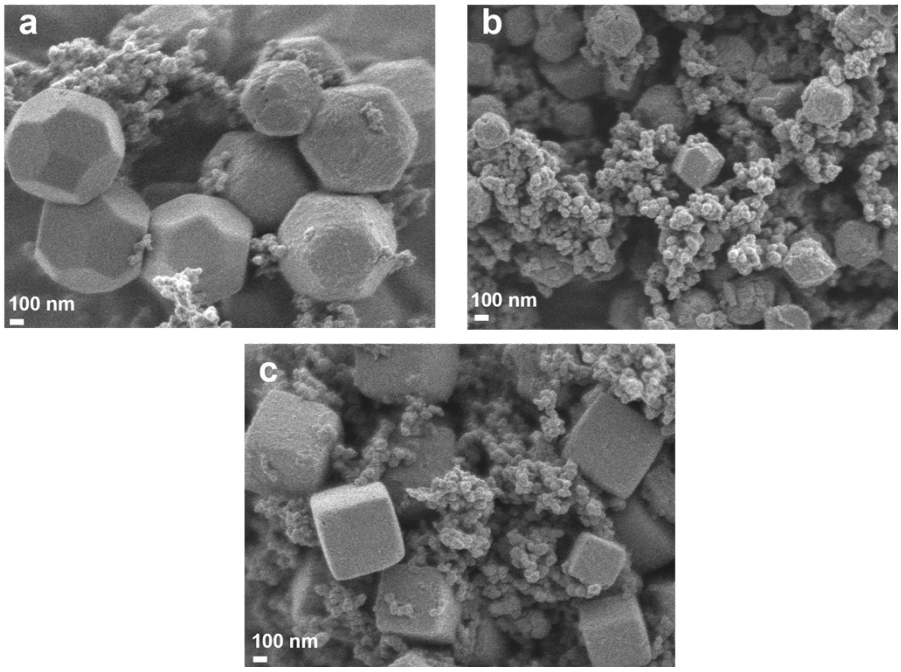

Fig. S9 SEM image of (a) bulk, (b) rhombic and (c) cubic after being used as a catalyst in ORR. Small particles observed in SEM are carbon black, which is added to MOF ink during the thin film preparation to increase the conductivity.

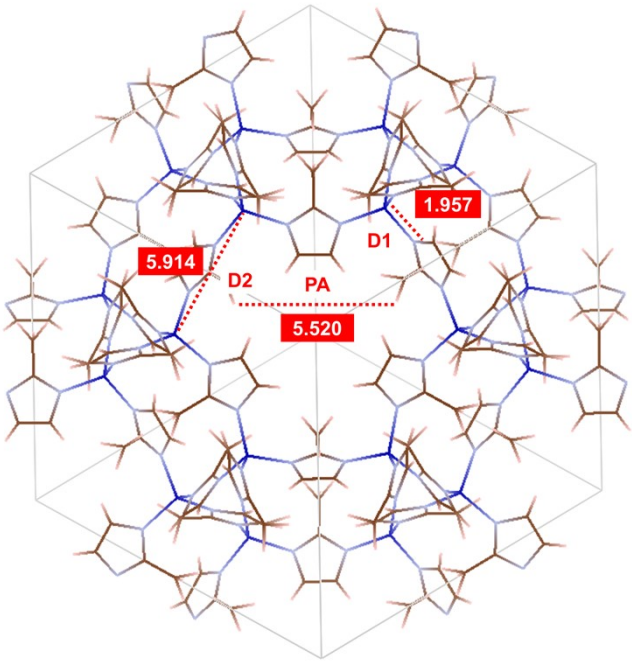

Fig. S10 Structural properties of bulk ZIF-67 with a crucial bond distance.

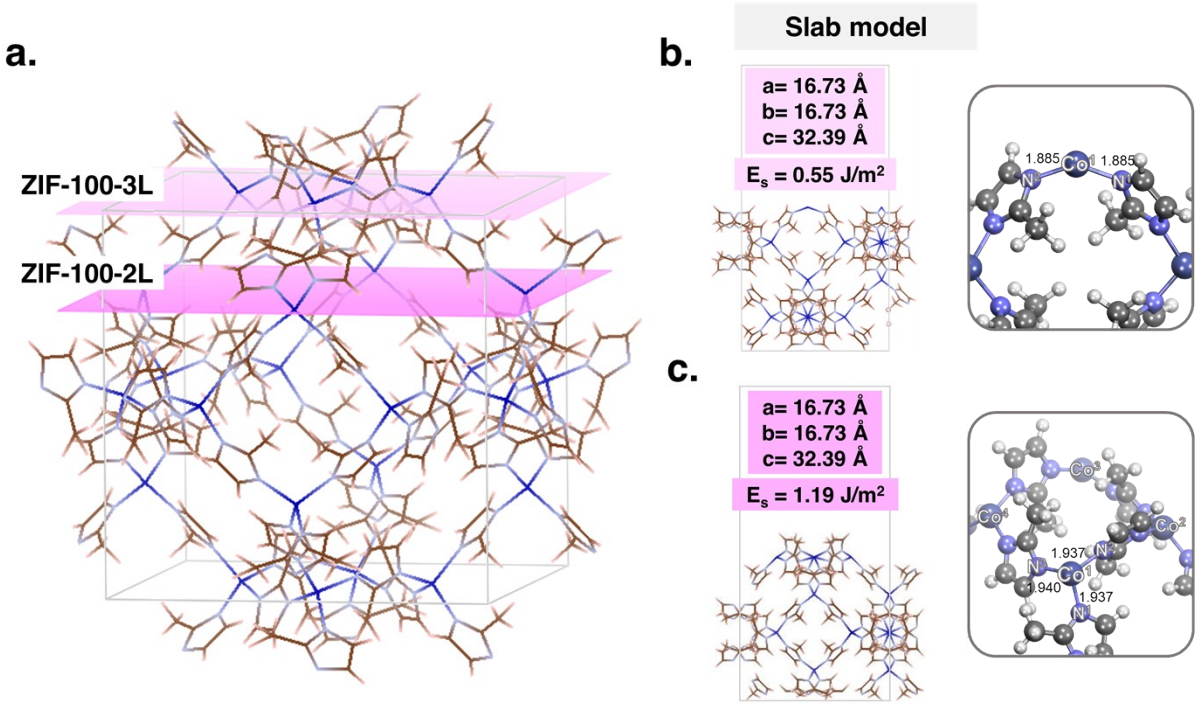

Fig. S11 (a.) Schematic representation of the exposed crystal facets in (b.) ZIF-100-2L and (c.) ZIF-100-3L facets.

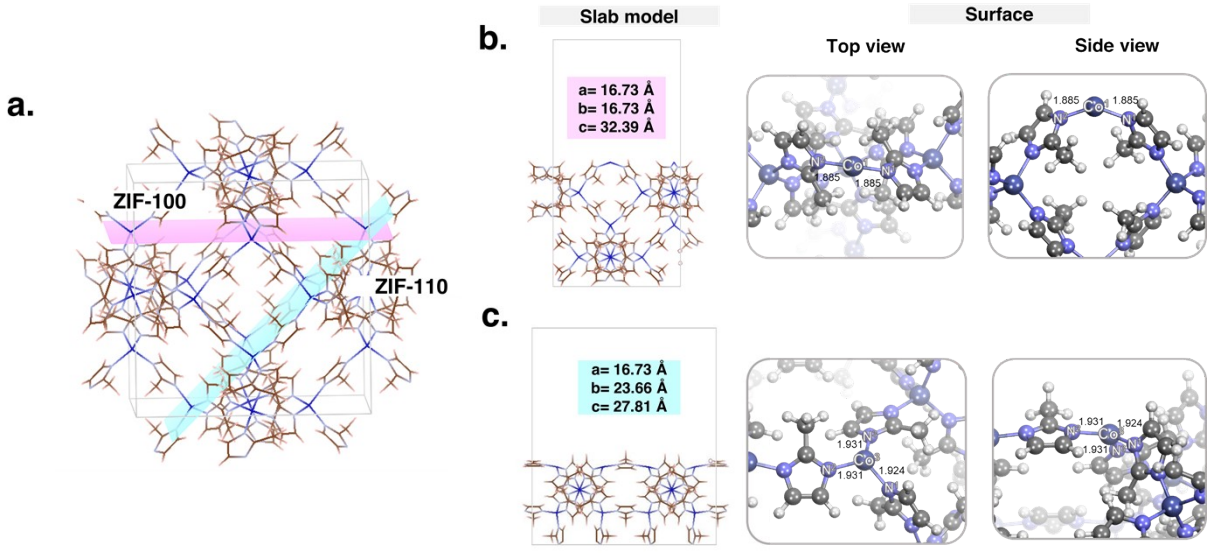

Fig. S12 (a.) Schematic representation of the exposed ZIF-67 crystal facets with different

facets representing the structural configuration of (b.) ZIF-100 and (c.) ZIF-110.

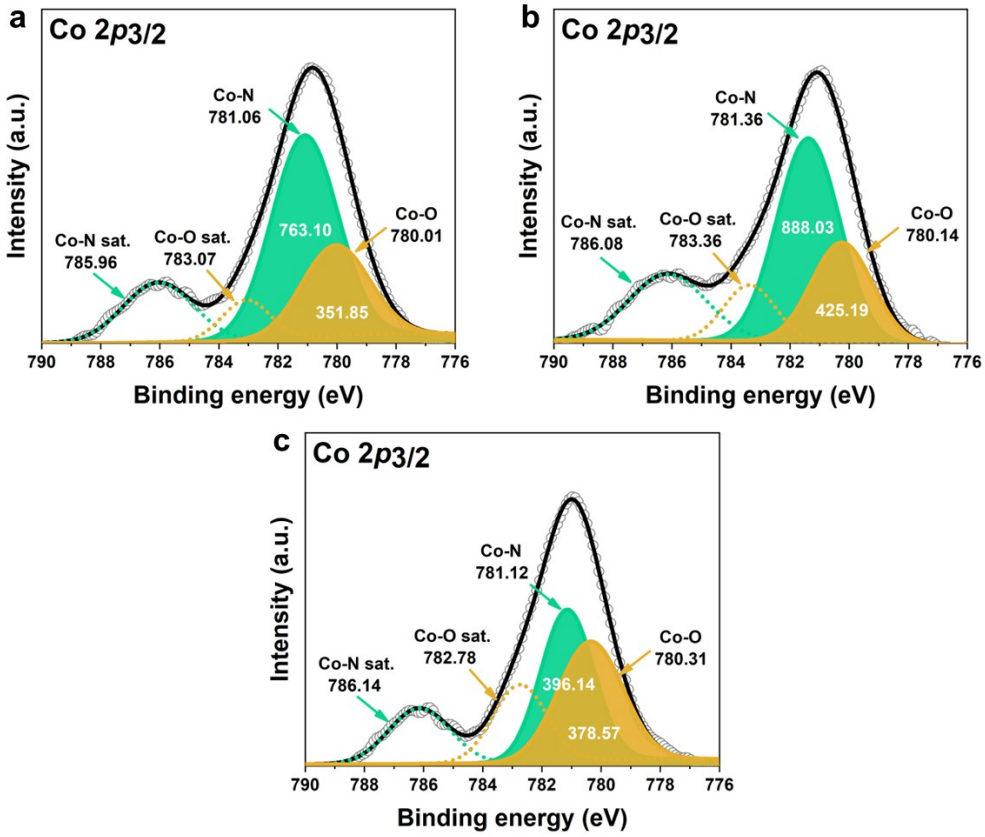

Fig. S13 XPS spectra of Co $2p_{3/2}$ of (a.) bulk ZIF-67 (b) rhombic ZIF-67 (c) cubic ZIF-67.

Table S1 The calculation of coordination number of all ZIF-67 samples from XPS

Sample	Area of Co-O	Area of Co-N	Number of Co-N*	Number of Ligand per metal center
Bulk	351.85	763.10	2.74	3
Rhombic (110)	425.19	888.03	2.70	3
Cubic (100)	378.57	396.14	2.04	2

*No of Co-N bond $= \dfrac{\text{Area of Co - N bond} \times \text{Maximum coordination number or 4}}{\text{Total area}}$

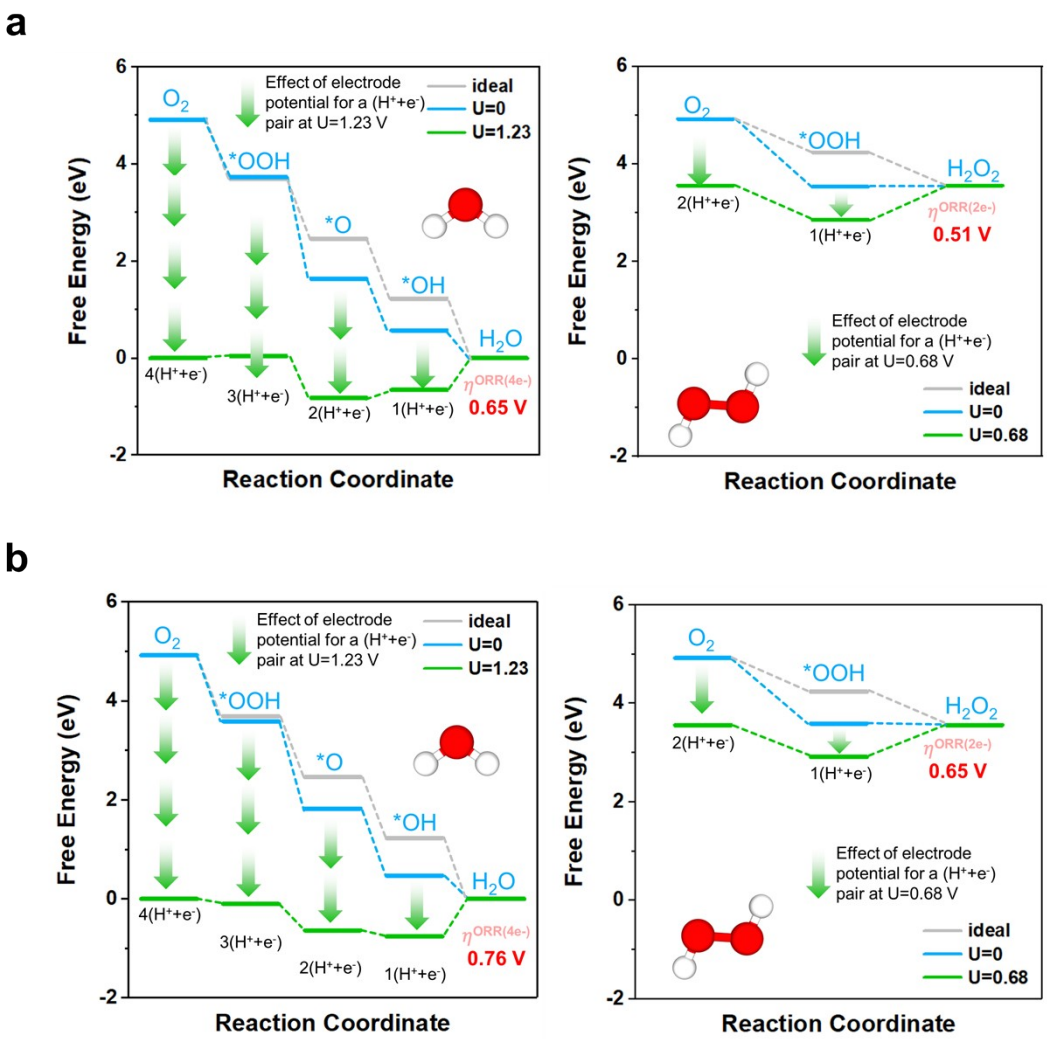

Fig. S14 The free energy diagrams of 4e- and 2e- ORR pathway of (a) ZIF-67 (100) (b) ZIF-67 (110) at U = 0 V and U = 1.23 V.

Table S2 Comparison of structural dimensions between ZIF-67 of previous and our work. D1, D2, and PA denote metal-nitrogen distance, metal-metal distance, and approximated pore aperture, respectively.

Bulk	D1 (Å)	D2 (Å)	PA (Å)	Unit cell (Å)
ZIF-8	1.979	5.969	5.567	16.881
ZIF-67	1.977	5.978	5.581	16.908
ZIF-67 (this work)	1.957	5.914	5.520	16.728

Table S3 The thermodynamic data for the molecules considered in this paper

Isolated gas	E (eV)	ZPE (eV)	TS (eV)	$\int C_p dT$ (eV)	Chemical potential	G (eV)
H_2	-6.77	0.27	0.40	0.09		-6.81
H_2O	-14.22	0.57	0.58	0.10	-0.09	-14.22

Our thermodynamic data for the molecules considered in this paper are corresponding to our previous works.[9-11]

Table S4 The overpotential of each ZIF-67 facet, Free energy adsorption, bond distance between surface and adsorbed species (d(Co-O)), Bader charge of Co (q(Co)) and adsorbed species (q(Species)). The negative and positive values stand for the accumulation and donation of electrons, respectively.

Plane	Overpotential (V)	Species	G_{ads}	d(Co-O)	q(Co)	q(Species)
100	0.65	OOH	3.73	1.809	1.13	-0.61
		O	1.64	1.679	1.23	-0.77
		OH	0.58	1.856	0.74	-0.60
110	0.76	OOH	3.59	1.828	0.67	-0.43
		O	1.82	1.684	1.26	-0.74
		OH	0.47	1.831	1.23	-0.55

References

1. G. Kresse and J. Hafner, *Phys. Rev. B.*, 1993, **47**, 558.
2. G. Kresse and J. Furthmüller, *Comput. Mater. Sci.*, 1996, **6**, 15-50.
3. G. Kresse and J. Furthmüller, *Phys. Rev. B.*, 1996, **54**, 11169.
4. J. P. Perdew, K. Burke and M. Ernzerhof, *Phys. Rev. Lett.*, 1996, **77**, 3865.
5. G. Kresse and D. Joubert, *Phys. Rev. B.*, 1999, **59**, 1758.
6. S. Grimme, J. Antony, S. Ehrlich and H. Krieg, *Chem. Phys.*, 2010, **132**, 154104.
7. H. T. Kwon, H.-K. Jeong, A. S. Lee, H. S. An and J. S. Lee, *J. Am. Chem. Soc.*, 2015, **137**, 12304-12311.
8. J. K. Nørskov, J. Rossmeisl, A. Logadottir, L. Lindqvist, J. R. Kitchin, T. Bligaard and H. Jónsson, *J. Phys. Chem. B.*, 2004, **108**, 17886-17892.
9. S. Chen, H. Yuan, S. I. Morozov, L. Ge, L. Li, L. Xu and W. A. Goddard, *J. Phys. Chem. Lett.*, 2020, **11**, 2541-2549.
10. C. Adhikari, A. Das and A. Chakraborty, *Mol. Pharm.*, 2015, **12**, 3158-3166.
11. Y. Ying, K. Fan, X. Luo, J. Qiao and H. Huang, *J. Mater. Chem. A*, 2021, **9**, 16860-16867.